Cluster Formation at Extreme Supersaturations
Nucleation versus Barrierless Transition

Kalikmanov, V. I.; Hagmeijer, R.

DOI
10.1021/acs.jpcb.9b09775

Publication date
2019

Document Version
Final published version

Published in
Journal of Physical Chemistry B

THE JOURNAL OF PHYSICAL CHEMISTRY B

Article

Cite This: J. Phys. Chem. B 2019, 123, 10890−10895

pubs.acs.org/JPCB

Cluster Formation at Extreme Supersaturations: Nucleation versus Barrierless Transition

V. I. Kalikmanov*[,†,‡,§] and R. Hagmeijer[†]

[†]Department of Engineering Fluid Dynamics, University of Twente, Drienerlolaan 5, 7522 NB Enschede, Netherlands

[‡]Twister Supersonic Gas Solutions, Einsteinlaan 10, 2289 CC Rijswijk, Netherlands

[§]Department of Geosciences, Delft University of Technology, Stevinweg 1, 2628 CN Delft, Netherlands

ABSTRACT: We study the process of cluster formation at extreme supersaturations and identify the temperature-supersaturation domain where evaporation can be neglected resulting in a barrierless process with kinetics dominated by the dimer formation. The cluster size distribution obeys the coalescence equation with the pressure−temperature-dependent association rate coefficients $k_{i,j}$. In view of the crucial role played by kinetics under these extreme conditions, the values of these coefficients calculated within the free molecular collision model are insufficient for the prediction of the nucleation rate and cluster distribution. An alternative is the use of $k_{i,j}$ obtained from the *ab initio* calculations. We apply these considerations to the analysis of recent water nucleation experiments in the postnozzle flow of a Laval nozzle. Theoretical predictions of nucleation rate are in an excellent agreement with experiment. At the same time, there is a discrepancy in the densities of small clusters. The latter can be attributed to the difference in $k_{i,j}$ extracted from the experimental data and those resulted from the *ab initio* calculations.

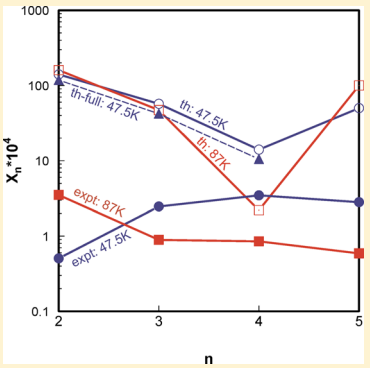

I. INTRODUCTION

The phenomenon of nucleation is associated with the nonequilibrium first-order phase transitions transforming a metastable parent phase to a thermodynamically stable daughter phase. The transformation proceeds through creation of small clusters (nuclei). Nucleation is ubiquitous in nature, playing an important role in a number of scientific fields ranging from atmospheric sciences to nanotechnology and medicine. In spite of the familiarity of these phenomena, accurate calculation of the nucleation rate and cluster distribution function for a number of practically relevant cases encounters serious difficulties. This is because the properties of small clusters are insufficiently well-known.

Classical nucleation theory (CNT), which has long been the most widely used theoretical model, fails to predict nucleation rates in situations when small, molecular-sized clusters play the leading role in the system's behavior. This shortcoming gave rise to a number of efforts aimed at understanding nucleation at the molecular level which requires taking into account intermolecular interactions (see ref 1 and references therein). One such model is the mean-field kinetic nucleation theory (MKNT)[2] which treats small clusters using statistical mechanical considerations and provides a smooth interpolation to the limit of big clusters obeying the classical capillarity approximation.

The majority of theoretical efforts refers to the development of thermodynamics of nucleation since the nucleation rate depends exponentially on the free energy barrier of cluster formation. Meanwhile, kinetics of nucleation, i.e., the rates of cluster formation and evaporation, in most studies remain the same as in the CNT. For the gas-to-liquid transition (condensation), the association rate in the CNT is described by the free molecular collisions based on the ideal gas kinetics. However, in the situations when the parent phase (vapor) is characterized by extremely high supersaturations, the vapor phase becomes unstable resulting in the disappearance of the nucleation barrier.[3] Under such conditions the role of kinetics of cluster formation becomes crucial, with the collisions rates being very sensitive to intermolecular interactions.

Among various substances for which nucleation has been studied theoretically and experimentally, water is of particular importance in view of the role played by water in various natural processes.

In recent experiments of Lippe et al.[4] formation of water clusters was studied in the uniform postnozzle flow of a Laval nozzle at flow temperatures T = 87 K and T = 47.5 K and extremely high supersaturations of ln S = 41 and ln S = 104, respectively. The cluster size distribution was measured using mass spectrometry after single-photon vacuum ultraviolet ionization. In the subsequent paper from the same group,[5] the results of these experiments were used to deduce the association rate coefficients of water molecules and to compare them with the results of *ab initio* calculations with the master equation approach of Bourgalais et al.[6]

In the present paper we undertake an opposite route: using theoretical considerations combined with *ab initio* collision rates,[6] we calculate the steady-state nucleation rate and cluster size distribution for the experimental conditions of ref 4.

Received: October 17, 2019
Revised: November 21, 2019
Published: November 22, 2019

DOI: 10.1021/acs.jpcb.9b09775
J. Phys. Chem. B 2019, 123, 10890−10895

The paper is organized as follows. In Section II we use the MKNT considerations to identify the domain of temperatures and supersaturations in which nucleation represents a barrierless process with kinetics dominated by the dimer formation and discuss the corresponding nucleation rate. In Section III we calculate the cluster distribution within this domain within the framework of the coalescence theory. Section IV is devoted to the analysis of water nucleation experiments of Lippe et al.[4] Calculations of the steady-state nucleation rate and cluster distribution with *ab initio* based association rate coefficients[6] are compared with experimental results.[4] Conclusions are summarized in Section V.

II. NUCLEATION AT HIGH SUPERSATURATIONS

The kinetics of cluster formation in nucleation theories is based on the Becker–Döring (BD) model[7] in which the evolution of clusters is considered as a sequence of elementary processes of attachment and detachment of monomers. According to the BD model, the rate of change of the n-cluster number density $\rho(n, t)$ with time t is balanced by the net fluxes *to* the n-clusters, $J(n-1, t)$, and *from* them, $J(n, t)$, as

$$\frac{\partial \rho(n, t)}{\partial t} = J(n-1, t) - J(n, t) \quad \text{for } n = 2, 3, \ldots$$

The cluster flux is constructed by considering the forward (*association*) rate, $f(n)$, and backward (*dissociation*) rate, $b(n)$

$$J(n, t) = f(n)\rho(n, t) - b(n+1)\rho(n+1, t)$$

The forward rate represents the number of collisions per unit time of vapor monomers with the surface of the cluster. The backward rate is determined from the detailed balance condition at equilibrium. CNT uses the notion of a *constrained equilibrium*, which would exist for a vapor at the same temperature T and the supersaturation $S > 1$ as the vapor in question.

An alternative, the *kinetic approach*, introduced by Katz and co-workers,[8] refers to the *true* equilibrium at liquid–vapor coexistence (saturation), corresponding to $S = 1$. Within this approach, which is particulary useful for the purposes of the present paper, $b(n)$ is determined from the detailed balance condition *at saturation* resulting in

$$b(n+1) = f_{\text{sat}}(n)\frac{\rho_{\text{sat}}(n)}{\rho_{\text{sat}}(n+1)} \tag{1}$$

where $\rho_{\text{sat}}(n)$ is the *cluster distribution function at saturation* at temperature T, and

$$f_{\text{sat}}(n) = \frac{f(n)}{S} \quad n = 1, 2, \cdots \tag{2}$$

is the forward rate at saturation; $b(n)$ is assumed to be independent of the vapor density. In the steady state, $J(n, t) = J$ with J being the steady-state nucleation rate. Within the kinetic approach[1]

$$J = \left[\sum_{n=1}^{\infty} \frac{1}{f(n)S^n\rho_{\text{sat}}(n)}\right]^{-1} \tag{3}$$

At a given T there exists a value of S beyond which the maximum of the Gibbs free energy of cluster formation $\Delta G(n)$ disappears, and so does the critical cluster corresponding to it. This happens at the so-called *pseudospinodal* $S_{\text{psp}}(T)$. The model for $S_{\text{psp}}(T)$ is based on the generalized Kelvin equation.[9] The height of the nucleation barrier ΔG^* at pseudospinodal is on the order of the energy of thermal fluctuations in the liquids: $\Delta G^* \approx k_B T$, where k_B is the Boltzmann constant. In what follows we consider the range of S higher than the pseudospinodal.

Let us rewrite eq 3 as

$$J^{-1} = \frac{1}{f(1)\rho_{\text{sat}}(1)S}\left[1 + \frac{f(1)\rho_{\text{sat}}(1)}{f(2)\rho_{\text{sat}}(2)S} + \frac{f(1)\rho_{\text{sat}}(1)}{f(3)\rho_{\text{sat}}(3)S^2} + \frac{f(1)\rho_{\text{sat}}(1)}{f(4)\rho_{\text{sat}}(4)S^3} + \ldots\right] \tag{4}$$

From eq 1

$$\frac{\rho_{\text{sat}}(1)}{\rho_{\text{sat}}(2)} = \frac{b(2)}{f_{\text{sat}}(1)}$$

$$\frac{\rho_{\text{sat}}(1)}{\rho_{\text{sat}}(3)} = \frac{\rho_{\text{sat}}(1)}{\rho_{\text{sat}}(2)}\frac{\rho_{\text{sat}}(2)}{\rho_{\text{sat}}(3)} = \frac{b(2)}{f_{\text{sat}}(1)}\frac{b(3)}{f_{\text{sat}}(2)}$$

...

Thus, for arbitrary $n > 1$

$$\frac{\rho(1)}{\rho_{\text{sat}}(n)} = \frac{b(2)}{f_{\text{sat}}(1)}\frac{b(3)}{f_{\text{sat}}(2)}\ldots\frac{b(n)}{f_{\text{sat}}(n-1)}$$

Combining this expression with eq 2 and substituting into eq 4, we find

$$J^{-1} = \frac{1}{f(1)\rho_{\text{sat}}(1)S}\left[1 + \frac{b(2)}{f(2)} + \frac{b(3)b(2)}{f(3)f(2)} + \frac{b(4)b(3)b(2)}{f(4)f(3)f(2)} + \ldots\right] \tag{5}$$

Within the purely phenomenological approach based on the capillarity approximation

$$\rho_{\text{sat}}^{\text{CNT}}(n) = \rho_{\text{sat}}^{\text{v}} e^{-\theta_\infty n^{2/3}} \tag{6}$$

where $\rho_{\text{sat}}^{\text{v}}(T)$ is the vapor number density at saturation. γ_∞ is the (macroscopic) surface tension; $\theta_\infty = \gamma_\infty s_1/(k_B T)$ is the *reduced* macroscopic surface tension. $s_1 = (36\pi)^{1/3}(\rho^{\text{l}})^{-2/3}$ is the "surface area of a monomer", and ρ^{l} is the number density of the liquid. An important feature of the CNT, particularly relevant for our considerations, is that eq 6 is valid for sufficiently big clusters and fails for small ones: for $n \to 1$ the macroscopic surface tension is not defined.

In order to treat all clusters on the same footing, we calculate $\rho_{\text{sat}}(n)$ using the MKNT.[1,2] Its main result states that within the mean-field approach $\rho_{\text{sat}}(n)$ is given by

$$\rho_{\text{sat}}(n) = \rho_{\text{sat}}^{\text{v}} e^{-\theta_{\text{micro}}[\overline{n^{\text{s}}}(n)-1]}$$

where $\overline{n^{\text{s}}}(n)$ is the average number of surface molecules in the n-cluster and $\theta_{\text{micro}}(T)$ is the reduced (in the units of $k_B T$) *free energy per surface particle*

$$\theta_{\text{micro}}(T) = -\ln\left(-\frac{B_2 p_{\text{sat}}}{k_B T}\right) \tag{7}$$

Here $p_{\text{sat}}(T)$ is the saturation vapor pressure, and $B_2(T)$ is the second virial coefficient. As seen from eq 7, θ_{micro} reflects

DOI: 10.1021/acs.jpcb.9b09775
J. Phys. Chem. B 2019, 123, 10890–10895

the nonideality of the vapor described by the second virial coefficient. The Gibbs free energy of n-cluster formation in MKNT is

$$\frac{\Delta G}{k_B T} \equiv g(n)_{T,S} = -n \ln S + \theta_{micro}[\overline{n^s}(n) - 1] \quad (8)$$

For small clusters $n \leq N_1$, where $N_1(T)$ is the coordination number in the liquid phase, $\overline{n^s}(n) = n$ yielding

$$\rho_{sat}(n) = \rho_{sat}^v e^{-\theta_{micro}(n-1)}$$

The backward rate eq 1 is then

$$b(n+1) = \left(\frac{e^{\theta_{micro}}}{S}\right) f(n)$$

In the present paper we consider the *XS-domain* of temperatures and supersaturations, satisfying the condition

$$r \equiv \frac{e^{\theta_{micro}}}{S} \ll 1 \quad (9)$$

For sufficiently low temperatures this also implies that

$$\ln S \gg 1 \quad (10)$$

For $n \geq N_1 + 1$, $\overline{n^s}(n)$ grows slower than $O(n)$ recovering the CNT behavior $\overline{n^s}(n) \sim n^{2/3}$ for big clusters (for details see ref 1, Chapter 7). In the XS-domain the contribution of clusters with $n \geq N_1 + 1$ to J is negligible: $g(n)$ is negative and monotonically decreases. Therefore, summation in eq 3 can be truncated at $n = N_1$. In eq 5, we have

$$\frac{b(j)}{f(j)} = r\frac{f(j-1)}{f(j)} \quad j = 2, ..., N_1 \quad (11)$$

The ratio of successive association rates in the right-hand side of this expression is $O(1)$ or less, so at $r \ll 1$

$$\frac{b(j)}{f(j)} \ll 1 \quad j = 2, ..., N_1$$

which implies that in the XS-domain evaporation can be neglected and cluster formation is a barrierless process with kinetics dominated by the dimer formation; its rate (eq 4) with the high degree of accuracy can be set to

$$J \approx \rho^v f(1) \quad (12)$$

where $\rho^v = \rho_{sat}(1)S$ is the vapor number density.

III. CLUSTER FORMATION IN THE XS-DOMAIN AS A COALESCENCE PROCESS

Considerations presented in the previous section show that in the XS-domain the nucleation process is purely kinetically driven (rather than thermodynamically driven) with dimer formation with the forward rate $f(1)$ being the critical step. Usually in the nucleation models $f(n)$ is found from the *ideal gas* kinetics:[10] since $f(n)$ enters the prefactor in the nucleation rate expression, its value is of minor importance compared to the exponential contribution of the free energy barrier. In the case of a barrierless transition, the situation is drastically different: an adequate quantitative prediction of the nucleation rate requires that $f(n)$ has to be found from the microscopic arguments taking into account intermolecular interactions.

Since evaporation rates for all cluster sizes are negligible, the growth of an arbitrary cluster is kinetically controlled by sequences of association (coalescence) processes. This observation is in line with the results of Monette and Klein[11] who considered the formation of nucleating droplets in the vicinity of the classical spinodal for the systems with long-range forces. Calculations based on the BD model and Monte Carlo simulations suggested that nucleation near spinodal represents a coalescence process.

According to coalescence (coagulation) theory,[12] the rate at which two single particles (droplets) of radii R_1 and R_2 collide to form doublets due to coalescence is proportional to the product of their number densities ρ_1 and ρ_2

$$J_{coal} = K(R_1, R_2)\rho_1\rho_2 \quad (13)$$

The coalescence kernel $K(R_1, R_2; T, p)$ with the dimensionality cm^3/s depends on particles' radii as well as on pressure and temperature. For equal-sized droplets of radius R and number density ρ, eq 13 reads $J_{coal} = K\rho^2$ with $K = K(R; T, p)$. According to eq 12 the steady-state nucleation rate is equal to the rate of coalescence of two monomers resulting in the dimer formation:

$$J \approx \rho^v f(1) = k_{1,1}(\rho^v)^2 \quad (14)$$

where the forward rate $f(1) = k_{1,1}\rho^v$. The quantity $k_{1,1}(T, p)$ represents the coalescence kernel for monomer−monomer association.

Within the framework of coalescence theory, the n-cluster is formed by association of i and $(n - i)$ clusters

$$(i) + (n-i) \rightarrow (n) \quad 1 \leq i \leq n-1$$

and disappears as a result of its association with other clusters in the system

$$(n) + (i) \rightarrow (n+i) \quad 1 \leq i \leq N_{max}$$

where N_{max} is the maximum cluster size. Evolution of $\rho(n, t)$ can be described by the discrete coalescence equation[12]

$$\frac{\partial\rho(n,t)}{\partial t} = \frac{1}{2}\sum_{i=1}^{n-1} k_{n-i,i}\rho(n-i,t)\rho(i,t) - \rho(n,t)\sum_{i=1}^{N_{max}} k_{i,n}\rho(i,t) \quad n = 2, 3, ..., N_{max} \quad (15)$$

where $k_{i,j}(T, p)$ is the temperature- and pressure-dependent kernel representing an *association rate coefficient* for $i - j$ cluster collisions. The first term in eq 15 describes the formation of an n-mer from coalescence of two smaller clusters: i-mer and $(n - i)$-mer. The second term describes the rate of depletion of the n-mer due to collisions with other clusters.

For the steady-state distribution $\rho_s(n) = \lim_{t\to\infty}\rho(n, t)$, eq 15 represents the system of $N_{max} - 1$ polynomial equations for $N_{max} - 1$ unknowns $\rho_s(2), ..., \rho_s(N_{max})$:

$$\frac{1}{2}\sum_{i=1}^{n-1} k_{n-i,i}\rho_s(n-i)\rho_s(i) - \rho_s(n)\sum_{i=1}^{N_{max}} k_{i,n}\rho_s(i) = 0 \quad n = 2, 3, ..., N_{max} \quad (16)$$

with $\rho_s(1) = \rho^v$. It is convenient to introduce the reduced cluster densities

$$X_i = \frac{\rho_s(i)}{\rho_s(1)} \leq 1 \quad i = 1, ..., N_{max}$$

DOI: 10.1021/acs.jpcb.9b09775
J. Phys. Chem. B 2019, 123, 10890−10895

and reduced association rate coefficients

$$a_{i,j} = \frac{k_{i,j}}{k_{1,1}} \quad i, j = 1, ..., N_{max}$$

Then, taking into account that $X_1 = a_{1,1} = 1$, eqs 16 take the form

$$(a_{1,n-1}X_{n-1} - a_{1,n}X_n) + \left[\frac{1}{2}\sum_{i=2}^{n-2} a_{n-i,i}X_{n-i}X_i - \sum_{i=2}^{N_{max}} a_{i,n}X_iX_n\right] = 0 \quad n = 2, 3, ..., N_{max} \tag{17}$$

The simplest approximation for X_i results from linearization of eqs 17 in X_i, implying the neglect of the terms in the square brackets, which yields

$$X_n \approx \frac{1}{a_{1,n}} = \frac{k_{1,1}}{k_{1,n}} \quad i = 1, ..., N_{max} \tag{18}$$

Physically this means that collisions of an arbitrary cluster with clusters other than monomers are excluded: thus, the n-cluster is formed by collision of an $(n - 1)$-cluster with a monomer and disappears, becoming the $(n + 1)$-cluster as a result of its collision with a monomer.

In CNT and its modifications, collision rates are described by the ideal gas kinetics. For the XS-domain, where cluster formation is a kinetically driven process, in order to calculate $k_{i,j}(T, p)$, one has to employ a more advanced approach taking into account intermolecular interactions. In particular, the association rate coefficients can be calculated using the *ab initio* transition state theory (TST).[13,14] By making the fundamental assumption of TST,[15] an inherently dynamic process can be characterized in terms of equilibrium statistical mechanical averages.[16]

IV. RESULTS: WATER NUCLEATION IN THE XS-DOMAIN

We apply considerations of the previous sections to the case of water nucleation in the postnozzle flow of a Laval nozzle at low temperatures and high supersaturations studied experimentally by Lippe et al.[4] Table 1 shows the values of the MKNT parameters for the experimental conditions.[4] Calculations are made using the same correlations for thermodynamic properties as in ref 4 (see Supporting Information there). It can be seen that both experimental points (T = 87 K, ln S = 41) and (T = 47.5 K, ln S = 104) fall in the XS-domain.

Table 1. MKNT Parameters for Water at the Conditions of Experiment[4]

T	N_1	θ_{micro}	ln S	$r(T, S)$
87 K	5	29.12	41	6.9×10^{-6}
47.5 K	5	60.84	104	1.8×10^{-19}

Figure 1 shows the behavior of the Gibbs free energy $g(n)$ for the experimental conditions.[4] The free energy is negative and decreases with n; beyond N_1, the decrease is much faster than for $n \leq N_1$.

In order to predict the steady-state nucleation rate and cluster distribution, one needs to know association rate coefficients $k_{i,j}(T, p)$. With this in mind we use the results of Bourgalais et al.[6] who performed *ab initio* calculations of $k_{i,j}(T, p)$ for water for the temperature range (20−100 K) and total pressures 10^{-6}−10 bar using the master equation approach.[17] The main idea behind this approach is coupling of the TST based evaluations of the microcanonical dissociation rate coefficients with simple models for collision induced energy transfer rates to obtain a master equation for the time dependence of the energy resolved state populations. The association rate coefficient, $k_{i,j}(T, p)$, is then obtained from the eigensolutions of this master equation. This approach requires potential energy values for the interaction between reactants at arbitrary separations and orientations, which are obtained via direct *ab initio* evaluations.

Experiments[4] were carried out for total pressures $p \approx 0.4$ mbar (with argon and nitrogen used as carrier gases) and temperatures T = 87 K and T = 47.5 K and thus fall within the pressure−temperature range of ref 6. Table 2 contains the values of $k_{1,n}(T, p)$ coefficients (n = 2, 3, 4, 5) from Table S3 of the Supplemental Material of the Bourgalais et al. paper.[6] Choosing the data set closest to the experiment,[4] we used the (100 K, 1 mbar) data for the T = 87 K experiment, and (50 K, 1 mbar) data for the T = 47.5 K experiment.

It is instructive to compare the values of $k_{1,n}$ from Table 2 with the corresponding values resulting from the free molecular collisions used in CNT:[1]

$$k_{1,n}^{CNT} = \frac{f(n)^{CNT}}{\rho^v} = \sqrt{\frac{k_BT}{2\pi m_1}}\, s_1 n^{2/3} \tag{19}$$

where $f(n)^{CNT}$ is the CNT forward rate based on free molecular collisions of monomers with n-clusters, and m_1 is the mass of a molecule of the condensable. Figure 2 illustrates this comparison for small clusters n = 1, ..., 5. While the free molecular ("CNT") values of $k_{1,n}$ slowly increase with n as $O(n^{2/3})$, the *ab initio* based values demonstrate essentially nonmonotonic behavior with the pronounced difference (about order of magnitude) between neighboring points. The *ab initio* dimerization rate coefficients $k_{1,1}$ for both experimental temperatures lie 2−3 orders of magnitude below the corresponding free molecular values. At the same time the *ab initio* collision rates of monomers with 4-mers, $k_{1,4}$, exceed the free molecular values.

A. Steady-State Nucleation Rate. In ref 4 the steady-state nucleation rate $J^{expt}(T, S)$ was determined by means of the time-dependent threshold (or Yasuoka−Matsumoto) method (known in molecular dynamics simulations) using the experimentally obtained cluster statistics. In the present paper we calculate the steady-state nucleation rate from eq 14 using the $k_{1,1}$ values from Table 2 and setting $\rho^v = p_{cond}/(k_BT)$, where p_{cond} is the partial pressure of the condensable (water). As can be seen from Table 3, theoretical predictions $J^{th}(T, S)$ are in an excellent agreement with experimental data $J^{expt}(T, S)$.

The steady-state nucleation rate found from eq 14 with the dimerization rates corresponding to free molecular collisions are 2−3 orders of magnitude higher than those presented in Table 3. This is an implication of the difference in $k_{1,1}$ values discussed earlier.

B. Steady-State Cluster Distribution. The accessible time scale for experiments[4] is on the order of a few hundred microseconds, while the steady state is achieved at $t_s \approx 50$ μs.[5] For the times larger than t_s we can apply the steady-state coalescence model of Section IV to calculate the cluster

DOI: 10.1021/acs.jpcb.9b09775
J. Phys. Chem. B 2019, 123, 10890−10895

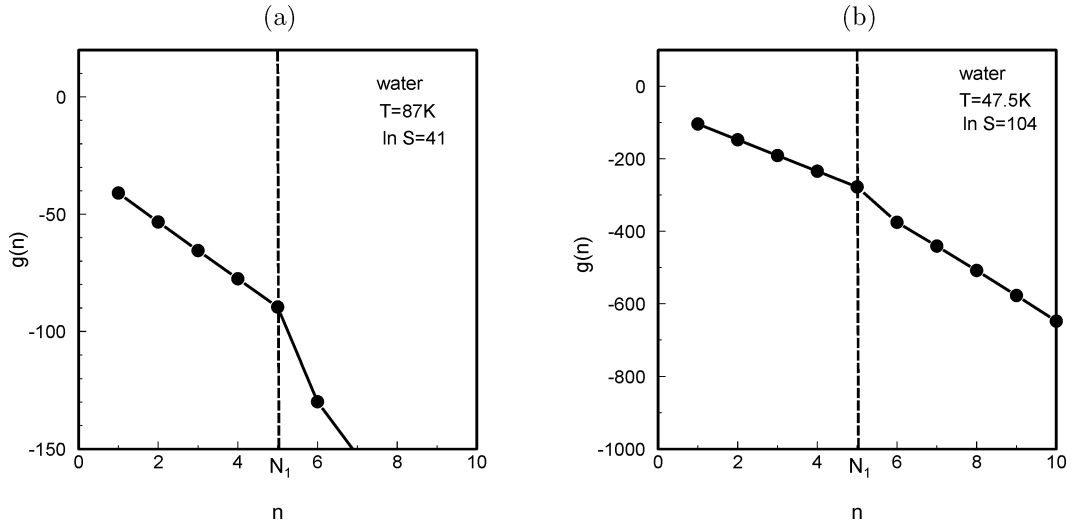

Figure 1. Gibbs free energy of cluster formation $g(n)$ for water nucleation corresponding to the experiment:[4] (a) T = 87 K, ln S = 41; (b) T = 47.5 K, ln S = 104.

Table 2. Association Rate Coefficients (cm^3/s) from the Supplemental Material for the Bourgalais et al. Paper[6] Approximately Corresponding to the Experimental Conditions of Reference 4[a]

	$k_{1,1}$	$k_{1,2}$	$k_{1,3}$	$k_{1,4}$	$k_{1,5}$
87 K expt	4.46×10^{-14}	2.84×10^{-12}	9.47×10^{-12}	1.98×10^{-10}	4.27×10^{-12}
47.5 K expt	8.72×10^{-13}	6.06×10^{-11}	1.54×10^{-10}	5.93×10^{-10}	1.73×10^{-10}

[a]The "87 K expt" line refers to the (T = 87 K, ln S = 41) experiment, and "47.5 K expt" refers to the (T = 47.5 K, ln S = 104) experiment.

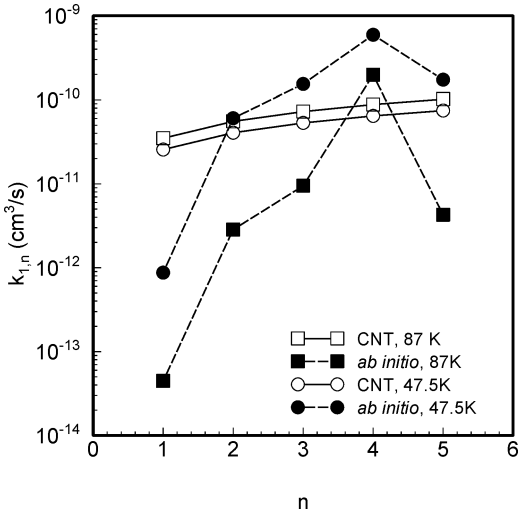

Figure 2. Association rate constants $k_{1,n}$, n = 1, ..., 5 for water corresponding to conditions of ref 4. Open symbols (CNT): free molecular collisions eq 19. Closed symbols (*ab initio*): simulation results of ref 6. Squares refer to the (T = 87 K, ln S = 41) experiment, and circles refer to the (T = 47.5 K, ln S = 104) experiment.[4]

Table 3. Steady-State Nucleation Rate for Experiments:[4] Theoretical Estimates According to Equation 14 (J^{th}) and Experimental Data (J^{expt})

	J^{th} (cm^{-3} s^{-1})	J^{expt} (cm^{-3} s^{-1})
T = 87 K, ln S = 41	3.2×10^{15}	$(4–5) \times 10^{15}$
T = 47.5 K, ln S = 104	4.6×10^{14}	2×10^{15}

distribution. [Note that in our terminology *coalescence* refers to collisions of *all* (i, j)-clusters in the system, whereas in ref 5 *coalescence* refers to collisions of clusters bigger than monomers (i > 1, j > 1)]. Figure 3 shows cluster statistics $X_n = \rho_s(n)/\rho_s(1)$ for small clusters obtained from the linearized model (eq 18) as well as the experimental data.[4,5]

To test the validity of the linearized model (eq 18), we also solved the full (nonlinearized) system of polynomial eq 17 for T = 47.5 K and N_{max} = 4:

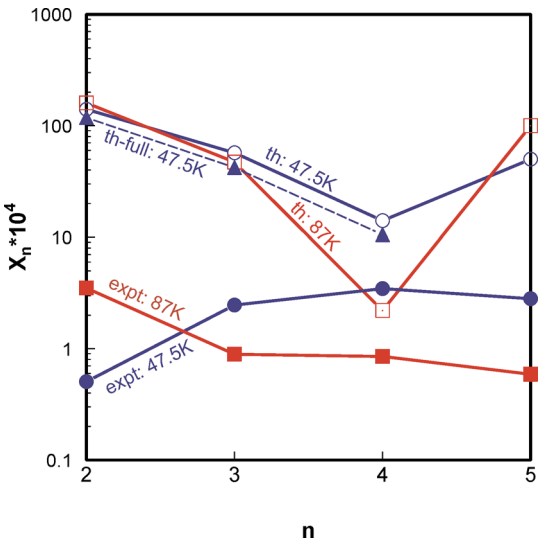

Figure 3. Reduced cluster densities $X_n = \rho_s(n)/\rho_s(1)$ for experimental conditions of ref 4 theoretical estimates using eq 18 ("th") and experimental data[4,5] ("expt"). Blue labels refer to T = 47.5 K, and red labels refer to T = 87 K. Also shown is the solution of the full system of polynomial coalescence eqs 20 for T = 47.5 K and N_{max} = 4: blue triangles labeled "th-full: 47.5 K". Lines are drawn to guide the eye.

DOI: 10.1021/acs.jpcb.9b09775
J. Phys. Chem. B 2019, 123, 10890−10895

$$1 - a_{1,2}X_2 = a_{2,2}X_2^2 + a_{2,3}X_2X_3 + a_{2,4}X_2X_4$$

$$a_{1,2}X_2 - a_{1,3}X_3 = a_{2,3}X_2X_3 + a_{3,3}X_3^2 + a_{3,4}X_3X_4$$

$$a_{1,3}X_3 - a_{1,4}X_4 = -\frac{1}{2}a_{2,2}X_2^2 + a_{2,4}X_2X_4 + a_{3,4}X_3X_4 + a_{4,4}X_4^2 \quad (20)$$

There is only one real solution X_2^{full}, X_3^{full}, X_4^{full} for this system (shown by triangles in Figure 3), belonging to the interval

$$0 < X_2^{\text{full}}, X_3^{\text{full}}, X_4^{\text{full}} < 1 \quad (21)$$

Its comparison with the linearized model (eq 18) reveals that the latter *overestimates* the exact solution (eq 21) by approximately 17−27%.

For T = 87 K the coalescence model predicts the decrease of cluster densities up to n = 4 followed by an increase at n = 5. Experimental data shows the decrease of densities for the whole range studied, $2 \leq n \leq 5$. The absolute values of densities differ by 1−2 orders of magnitude except for n = 4 where they differ by a factor of 3. For T = 47.5 K the model results and experimental data are qualitatively different. While theoretical predictions show the same trend as for T = 87 K, experimental densities demonstrate an *increase* up to n = 4 followed by a slight decrease at n = 5. The absolute values of densities differ by 1−2 orders of magnitude except for n = 4 where they differ by a factor of 4.

These discrepancies are due to the difference in the values of the association rate coefficients $k_{1,n}$ extracted from the experimental data, as discussed in ref 5 and those resulting from the *ab initio* calculations.[6]

V. CONCLUSION

In the present paper we studied the cluster formation at extreme supersaturations and showed that in the XS-domain eq 9 evaporation can be neglected and cluster formation is a barrierless process with kinetics dominated by the dimer formation. We showed that the cluster distribution function obeys the coalescence equation with the pressure−temperature-dependent coalescence kernels. Since the collision processes are dominated by collisions of various clusters with monomers, one can derive the cluster distribution from the linearized coalescence model. The steady-state solution of this simplified model is given by eq 18.

In view of the crucial role played by kinetics at these conditions, the association rate coefficients found from the free molecular (ideal gas) collision model are insufficient to predict nucleation rate and cluster distribution. A better alternative is the use of association rate coefficients from the *ab initio* calculations.

We applied these considerations to the analysis of water nucleation in the postnozzle flow of a Laval nozzle at high supersaturations experimentally studied by Lippe et al.[4] For the association rate coefficients $k_{i,j}$ the values found in the *ab initio* calculations of Bourgalais et al.[6] were used. Theoretical predictions of nucleation rate are in an excellent agreement with experiment. At the same time there is a discrepancy in the densities of small clusters between the model and experiment.[4] The latter can be attributed to the difference in the values of $k_{1,n}$ extracted from the experimental data, and the corresponding *ab initio* results.

We thank Prof. Ruth Signorell and Dr. Martina Lippe for stimulating discussions and for sending us the experimental data on cluster distribution prior to publication.

AUTHOR INFORMATION

Corresponding Author

*E-mail: Vitaly.Kalikmanov@twisterbv.com.

ORCID

V. I. Kalikmanov: 0000-0001-6626-287X

Notes

The authors declare no competing financial interest.

REFERENCES

(1) Kalikmanov, V. I. *Nucleation Theory*; Springer: Dordrecht, 2013.
(2) Kalikmanov, V. I. Mean-field Kinetic Nucleation Theory. *J. Chem. Phys.* **2006**, *124*, 124505.
(3) Vehkamäki, H.; Riipinen, I. Thermodynamics and Kinetics of Atmospheric Aerosol Particle Formation and Growth. *Chem. Soc. Rev.* **2012**, *41*, 5160−5173.
(4) Lippe, M.; Chakrabarty, S.; Ferreiro, J.; Tanaka, K.; Signorell, R. Water Nucleation at Extreme Supersaturation. *J. Chem. Phys.* **2018**, *149*, 244303.
(5) Li, C.; Lippe, M.; Krohn, J.; Signorell, R. Extraction of Monomer-Cluster Association Rate Constants from Water Nucleation Data Measured at Extreme Supersaturations. *J. Chem. Phys.* **2019**, *151*, No. 094305.
(6) Bourgalais, J.; Roussel, V.; Capron, M.; Benidar, A.; Jasper, A. W.; Klippenstein, S. J.; Biennier, L.; Le Picard, S. D. Low Temperature Kinetics of the First Steps of Water Cluster Formation. *Phys. Rev. Lett.* **2016**, *116*, 113401.
(7) Becker, R.; Döring, W. Kinetische Behandlung der Keimbildung in übersättigten Dämpfern. *Ann. Phys. (Leipzig)* **1935**, *416*, 719−752.
(8) Katz, J. L.; Wiedersich, H. Nucleation Theory Without Maxwell Demons. *J. Colloid Interface Sci.* **1977**, *61*, 351−355.
(9) Kalikmanov, V. I. Generalized Kelvin Equation and Pseudospinodal in Nucleation Theory. *J. Chem. Phys.* **2008**, *129*, No. 044510.
(10) Landau, L. D.; Lifshitz, E. M. *Statistical Physics*; Pergamon: Oxford, 1969.
(11) Monette, L.; Klein, W. Spinodal Nucleation as a Coalescence Process. *Phys. Rev. Lett.* **1992**, *68*, 2336−2339.
(12) Seinfeld, J. H. *Atmospheric Chemistry and Physics of Air Pollution*; J. Wiley & Sons: New York, 1986.
(13) Johnston, H. S. *Gas Phase Reaction Rate Theory*; Ronald: New York, 1966.
(14) Gilbert, R.; Smith, S. C. *Theory of Unimolecular and Recombination Reactions*; Blackwall: Oxford, 1990.
(15) Wigner, E. The Transition State Method. *Trans. Faraday Soc.* **1938**, *34*, 29−41.
(16) Schenter, G. K.; Kathmann, S. M.; Garrett, B. C. Variational Transition State Theory of Vapor Phase Nucleation. *J. Chem. Phys.* **1999**, *110*, 7951−7959.
(17) Miller, G. A.; Klippenstein, S. J. Master Equation Methods in Gas Phase Chemical Kinetics. *J. Phys. Chem. A* **2006**, *110*, 10528−10544.

DOI: 10.1021/acs.jpcb.9b09775
J. Phys. Chem. B 2019, 123, 10890−10895